JSR Publications

Available Online

J. Sci. Res. **18** (2), 309-330 (2026)

JOURNAL OF SCIENTIFIC RESEARCH

www.banglajol.info/index.php/JSR

Groundwater Contamination and Public Health Concerns: Nitrate and Fluoride Toxicity in GHMC of Hyderabad, Telangana State, India

A. Pallavi [*], **A. Edukondal**[1]

Department of Geology, Osmania University, Hyderabad, Telangana State, India, 500007

Received 2 November 2025, accepted in final revised form 13 March 2026

Abstract

This study evaluates hydrogeochemical processes and associated health risks from nitrate and fluoride contamination in shallow hard-rock aquifers of the semi-arid Greater Hyderabad Municipal Corporation (GHMC) region, Telangana, South India. A total of 44 groundwater samples were collected during the pre- and post-monsoon seasons of 2023. Spatial analysis showed elevated nitrate levels in the south-western, northern, and central areas, with 36 % (pre-monsoon) and 40 % (post-monsoon) of samples exceeding the permissible limit (45 mg/L). Fluoride concentrations were high in the northern, southern, and south-western zones, where 64 % and 59 % of samples exceeded the acceptable limit (1.0 mg/L) during pre- and post-monsoon periods, respectively. Gibbs diagrams indicated that rock–water interaction and evaporation are the dominant processes controlling groundwater chemistry. Statistical and factor analyses revealed feldspar weathering, cation exchange, and combined geogenic and anthropogenic influences. Health risk assessment showed hazard quotient values (>1.0) for both contaminants, with children more vulnerable than adults. The results emphasize the need for regular monitoring and sustainable groundwater management in the GHMC region.

Keywords: Health risk assessment; Fluoride and nitrate; Piper; Gibb's; Hazard quotient.

doi: https://dx.doi.org/10.3329/jsr.v18i2.85390 J. Sci. Res. 18 (2), 309-330 (2026)

1. Introduction

Human survival is fundamentally dependent on natural resources, among which clean air and safe water are indispensable. Groundwater and surface water constitute the primary freshwater resources for domestic, agricultural, and industrial activities worldwide [1]. In arid and semi-arid regions, where surface water availability is limited, groundwater serves as the principal source of potable water for nearly one-third of the global population [2]. However, groundwater quality has been increasingly compromised due to a combination of natural hydrogeochemical processes and anthropogenic activities, resulting in water scarcity and associated environmental and public health challenges [3,4].

Among various groundwater contaminants, nitrate and fluoride have received significant attention over the past two decades owing to their widespread occurrence and potential health risks. Elevated concentrations of nitrate in groundwater are commonly attributed to

[*]*Corresponding author*: achirajupallu@gmail.com

agricultural runoff, excessive application of nitrogen-based fertilizers, poorly designed septic systems, leakage from urban drains, slaughterhouses, dairy and poultry farms, and improper disposal of human and animal wastes [5-8]. Consequently, high nitrate levels are frequently reported in intensively cultivated agricultural lands and densely populated urban and peri-urban areas [9,10].

Fluoride contamination in drinking water is a major cause of dental and skeletal fluorosis, affecting millions of people worldwide. In India, fluorosis has been reported in 28 states, impacting approximately 66 million people [11]. Elevated fluoride concentrations are primarily controlled by the dissolution of fluoride-bearing minerals such as fluorite, hornblende, biotite, and apatite, particularly in granitic and gneissic terrains [12]. Previous studies have also highlighted the role of anthropogenic factors, including the excessive use of fertilizers and pesticides, in enhancing fluoride mobility in groundwater systems [13]. Health risk assessments indicate that children are more vulnerable to non-carcinogenic risks associated with nitrate and fluoride exposure than adults due to lower body weight and higher intake rates [14].

Groundwater quality deterioration has further been influenced by climatic variability, prolonged water–rock interaction, poor drainage conditions, and seasonal recharge processes, especially in semi-arid regions dominated by crystalline lithology [15,16]. In recent years, increasing concern has been raised regarding the adverse impacts of long-term consumption of nitrate- and fluoride-rich groundwater on human health. To address these concerns, several guidelines, regulatory standards, and human health risk assessment (HRA) models have been developed to evaluate exposure through ingestion pathways [2,17–19]. These approaches have been widely adopted to quantify potential health risks and to support groundwater quality management strategies.

Hyderabad district, one of the 33 districts of Telangana State, southern India, has experienced rapid urbanization, industrial development, and population growth over the past few decades. The region is characterized by a semi-arid climate and is underlain predominantly by granitic rocks. Intensive groundwater abstraction combined with increasing anthropogenic pressures has resulted in notable deterioration of groundwater quality, raising serious concerns regarding its suitability for drinking purposes. The present study aims to (i) evaluate the spatio-temporal distribution of nitrate and fluoride in groundwater, (ii) identify the hydrogeochemical processes governing their enrichment, and (iii) assess potential non-carcinogenic health risks using the Total Hazard Index (THI). The findings of this study provide critical insights into vulnerable zones and contribute to the development of effective groundwater management and public health protection strategies.

2. Materials and Methods

2.1. *The study area*

The Greater Hyderabad Municipal Corporation (GHMC) region extends between latitudes 17.3160º–17.5300º N and longitudes 78.2702º–78.6110º E (Fig. 1), covering a total area of about 210 km². The study area is predominantly composed of rocky terrain with monolithic

rock outcrops along its outskirts. The mean annual rainfall recorded between 2018 and 2023 is 866 mm (Table 1; Fig. 2). Seasonal distribution of rainfall indicates that 57 % occurs during the southwest monsoon, 10 % during the northeast monsoon, 0.4 % in winter, and 33% in summer. The mean monthly rainfall variation is illustrated in Table 1 and Fig. 2.

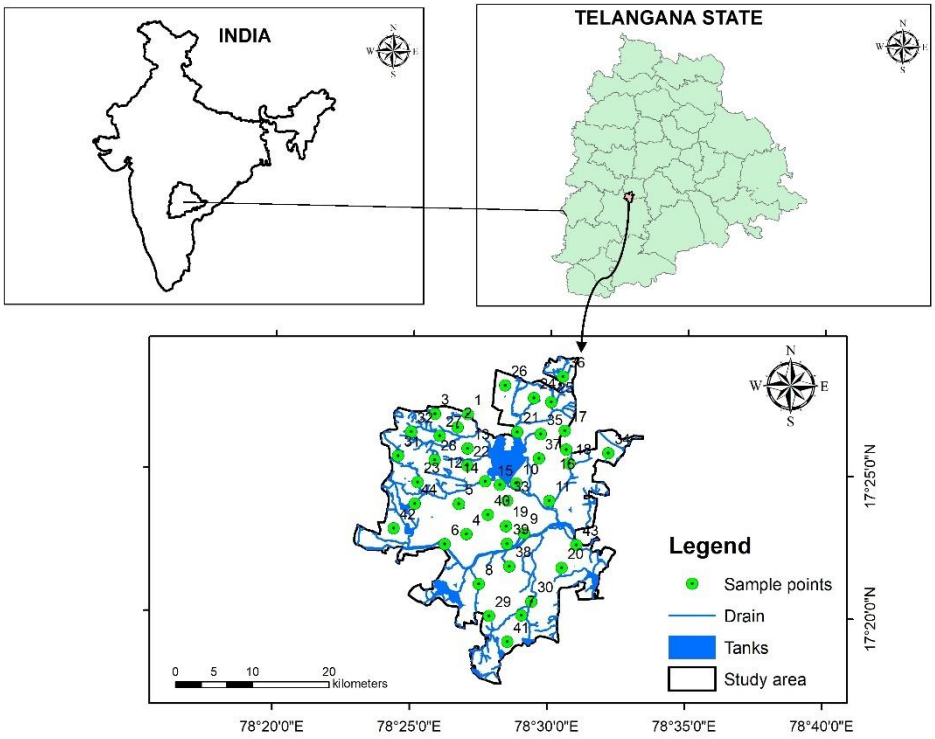

Fig. 1. Study area with sample points.

2.2. *Sample collection*

To assess groundwater quality, a total of 44 water samples were collected from different locations in and around Greater Hyderabad Municipality Corporation of Hyderabad District, Telangana State, India, during the pre-monsoon (May 2023) and post-monsoon (December 2023) seasons. Sampling was carried out using pre-cleaned one-liter polyethylene bottles, which were acid-washed with 1:1 dilute nitric acid and rinsed thoroughly with distilled water. Prior to collection, the bottles were rinsed again with the respective groundwater sample to avoid contamination. In the field, pH and electrical conductivity (EC) were measured immediately using a portable pH/EC meter (Hanna Instruments, USA, Model H-198130). Total dissolved solids (TDS) were calculated from EC values using a conversion factor of 0.64. In addition to pH and EC, major cations and anions were analyzed following the standard procedures recommended by APHA [20]

(Table 1). The complete statistical summary of groundwater chemistry for the study area is presented in Table 2.

Table 1. Standard procedure of major ions of groundwater in the study area, BIS [24].

Parameter	Method, instrument (make)	Reagents
pH	pH/EC meter (Hanna)	pH 4, 7 and 9.2 (buffer tablets)
EC (µS/cm)	pH/EC meter (Hanna)	Potassium chloride (KCl)
TDS (mg/L)	EC x 0.64	Calculation
TH as $CaCO_3$ (mg/L)	Titrimetric	Hydrochloric Acid (HCl) and Standard EDTA solution
Ca^{2+} (mg/L)	Titrimetric with EDTA	EDTA, Sodium hydroxide (NaOH) and Murexide
Mg^{2+} (mg/L)	TH-Ca^{2+}	Calculation
Na^{+} (mg/L)	Flame photometer (Elico) (Systronics, 128)	Sodium chloride (NaCl), KCl and Calcium carbonate ($CaCO_3$)
K^{+} (mg/L)	Flame photometer (Elico) (Systronics, 128)	Sodium chloride (NaCl), KCl and Calcium carbonate ($CaCO_3$)
HCO_3^{-} (mg/L)	Titrimetric	Hydrosulfuric acid (H_2SO_4), Methyl orange
Cl^{-} (mg/L)	Titrimetric	Silver nitrate, Potassium chromate
SO_4^{2-} (mg/L)	UV-Visible spectrophotometer (Spectronic 21, BAUSCH and LOMB)	Glycerol, HCl, ethyl alcohol, NaCl, $BaCl_2$, sodium sulphate
NO_3^{-} (mg/L)	UV-Visible spectrophotometer (Spectronic 21, BAUSCH and LOMB)	Brucine-sulpanilic acid, KNO_3 and H_2SO_4
F^{-} (mg/L)	Ion Selective Electrode, (Orion analyzer)	TISSB- III, F stock solution

Table 2. Statistical summary of groundwater chemistry of the study area.

Variables	Pre-monsoon season				Post-monsoon season				BIS [24]
	Minimum	Maximum	Mean	% of samples exceeded the limits	Minimum	Maximum	Mean	% of samples exceeded the limits	
pH	6.85	8.96	8.04	23	6.76	8.52	7.54	2	6.5 - 8.5
EC (µS/cm)	495	2990	1305		390	4860	1445	-	-
TDS (mgL)	317	1914	835	95	250	3110	925	86	500
Ca^{2+} (mg/L)	16	496	76	30	32	488	120	57	75
Mg^{2+} (mg/L)	5	78	38	52	10	214	120	36	30
TH as $CaCO_3$	140	1280	344	75	148	1340	406	84	200
Na^{+} (mg/L)	40	444	144	-	24	342	140	-	-
K^{+} (mg/L)	1	21	5	-	1	23	4	-	-
CO_3^{-} (mg/L)	0	60	11	-	0	48	3	-	-
HCO_3^{-} (mg/L)	77	638	266	-	55	622	342	-	-
Cl^{-} (mg/L)	30	720	211	27	40	1050	216	25	250
NO_3^{-} (mg/L)	3	230	56	36	5	797	63	40	45
SO_4^{2-} (mg/L)	6	120	31	-	9	66	34	-	200
F^{-} (mg/L)	0.21	3.03	1.20	64	0.28	5.94	1.28	59	1.5
Gibb's I	0.22	0.79	0.53	-	0.18	0.93	0.46	-	-
Gibb's II	0.15	0.90	0.62	-	0.19	0.89	0.51	-	-

2.3. *Geology*

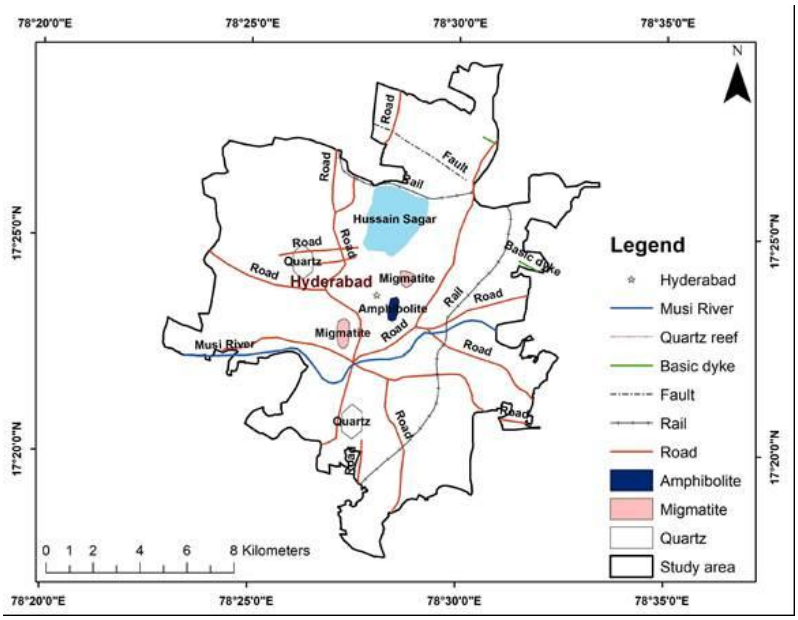

Fig. 2. Geology map of the study area.

The topography of the study area is relatively uniform and is underlain by Precambrian granites, predominantly pink and grey varieties. The region is frequently traversed by bodies of dolerites, gneisses, amphibolites, epidote, pegmatite, aplite, and quartz veins. Granitic rocks dominate the terrain and are composed mainly of feldspars rich in calcium, sodium, and potassium. Accessory minerals such as fluorite, apatite [$Ca_5(PO_4)_3(F,Cl,OH)$], hornblende [$Ca_2(Mg,Fe, Al)_5(Al, Si)_8O_{22}(OH)_2$], and biotite [$K(Mg,Fe)_3(AlSi_3O_{10})(F,OH)_2$] contribute significantly to the release of fluoride into the groundwater system. In addition, intrusive dolerite dykes are particularly prominent in the northern and western parts of the region, forming key structural features that influence groundwater movement. The aquifer system is further controlled by joints: vertical joints act as conduits facilitating groundwater percolation, while horizontal joints maintain lateral continuity of the aquifer [19] (Fig. 2).

2.4. *Health Risk Assessment (HRA)*

In this study, human health risk assessment was carried out considering exposure through the drinking water pathway [21,22]. Chronic daily intake of groundwater was identified as the primary exposure route for nitrate (NO_3^-) and fluoride (F^-). The non-carcinogenic risk associated with these contaminants was evaluated using the hazard quotient (HQ), following the guidelines and recommended standards of the US Environmental Protection Agency [3].

$$ADD = \frac{CGW \times IR \times ED \times EF}{ABW \times AET}$$

The average daily dose (ADD) of nitrate (NO_3^-) and fluoride (F^-) through drinking water ingestion was calculated using standard risk assessment guidelines. In this equation, represents the concentration of the contaminant in groundwater (mg/L). The ingestion rate (IR) was considered as 2.5 L/day for adults and 0.78 L/day for children. The exposure duration (ED) was taken as 70 years for adults and 6 years for children, while the exposure frequency (EF) was expressed in days per year. The average body weight (ABW) was assumed to be 65 kg for adults and 15 kg for children. The average exposure time (AET) expressed in days and was considered as 25,550 days for adults and 2,190 days for children. Accordingly, the ADD values were estimated in mg/kg/day for both age groups.

$$HQ = \frac{ADD}{RfD}$$

The non-carcinogenic for total hazard quotient is denoted as HQ and the reference dose of fluoride and nitrate 0.06 mg/kg-day and 1.6 mg/kg-day, respectively [23].

3. Results and Discussion

3.1. *Hydrochemical framework of groundwater*

The chemical composition of groundwater in the study area was examined in relation to the drinking water quality criteria recommended by the Bureau of Indian Standards (BIS) [24] (Table 2). Groundwater samples exhibited pH values ranging from 8.04 during the pre-monsoon to 7.54 during the post-monsoon season, indicating predominantly alkaline conditions. Exceedance of the recommended pH range (6.5-8.5) was observed in 23 % of pre-monsoon samples, while only 2 % of post-monsoon samples are excess the permissible limits. Electrical conductivity (EC), which reflects the total ionic strength of groundwater, showed average values of 1305 µS/cm in the pre-monsoon and 1445 µS/cm in the post-monsoon season (Table 2). The relatively higher post-monsoon EC suggests enhanced dissolution of aquifer minerals following recharge processes.

3.2. *Major cations*

Calcium concentrations varied from 14 to 496 mg/L in the pre-monsoon and from 32 to 488 mg/L in the post-monsoon season (Table 2). A significant proportion of groundwater samples exceeded the BIS acceptable limit of 75 mg/L, accounting for 76 % in the pre-monsoon and 57 % in the post-monsoon period [24]. Such elevated calcium levels are primarily controlled by the breakdown of calcium-bearing plagioclase feldspars abundant in the granitic lithology [22].

Magnesium concentrations ranged between 5–78 mg/L during the pre-monsoon and 10–214 mg/L during the post-monsoon season. Exceeded the permissible limit of 30 mg/L was observed in 52 % of pre-monsoon and 36 % of post-monsoon samples. The enrichment of magnesium is attributed to silicate mineral weathering and ion-exchange reactions operating within the fractured granitic aquifer system.

Sodium levels in groundwater ranged from 40 to 444 mg/L during the pre-monsoon and from 24 to 342 mg/L during the post-monsoon, whereas potassium concentrations remained comparatively low, varying from 1 to 21 mg/L and 1 to 23 mg/L in the respective seasons (Table 2). The subdued potassium concentrations are likely due to its strong retention within clay minerals and feldspar structures.

3.3. *Major anions*

Carbonate concentrations ranged from 0 to 60 mg/L in the pre-monsoon and from 0 to 48 mg/L in the post-monsoon period. Bicarbonate exhibited higher concentrations, varying between 77 and 638 mg/L during the pre-monsoon and 55 to 622 mg/L during the post-monsoon season (Table 2), reflecting active carbonate weathering and CO_2-driven reactions.

Chloride concentrations displayed wide spatial and seasonal variability, ranging from 30 to 710 mg/L in the pre-monsoon and from 40 to 1050 mg/L in the post-monsoon season. Based on BIS guidelines [24], 27 % of pre-monsoon and 25 % of post-monsoon samples exceeded the permissible limit of 250 mg/L. Elevated chloride levels are interpreted as the combined influence of natural sources, including weathering of chloride-bearing minerals such as apatite, and anthropogenic inputs from urban wastewater and industrial discharges infiltrating the aquifer [25].

Sulphate concentrations ranged from 6 to 120 mg/L during the pre-monsoon and from 9 to 66 mg/L during the post-monsoon period. All samples remained well within the acceptable drinking water limit of 200 mg/L prescribed by BIS [24].

The relative abundance of dissolved ions followed the sequence $Ca^{2+} > Na^{+} > Mg^{2+} > K^{+}$ among cations and $Cl^{-} > HCO_3^{-} > NO_3^{-} > SO_4^{2-} > F^{-}$ among anions in both hydrological seasons.

Total dissolved solids (TDS) concentrations ranged from 317 to 1914 mg/L during the pre-monsoon and from 390 to 4860 mg/L during the post-monsoon season (Table 2). According to BIS drinking water standards [24], the majority of samples (95 % in pre-monsoon and 86 % in post-monsoon) exceeded the recommended limit of 500 mg/L. Based on the classification proposed by Davis and De Wiest [26] and Freeze and Cherry [27], groundwater was categorized as fresh (75 %) and brackish (25 %) during the pre-monsoon, and fresh (73 %) and brackish (27 %) during the post-monsoon season (Table 3). Elevated TDS levels may adversely affect human health by inducing gastrointestinal discomfort and laxative effects [28].

Total hardness (expressed as $CaCO_3$) ranged from 140 to 1280 mg/L in the pre-monsoon and from 148 to 1340 mg/L during the post-monsoon season (Table 2). Exceeded of the BIS permissible limit of 200 mg/L was recorded in 75 % of pre-monsoon and 84 % of post-monsoon samples [24]. Using the classification scheme of Sawyer and McCarty [29], groundwater samples were grouped as moderately hard (18 %), hard (39 %), and very hard (43 %) during the pre-monsoon, and moderately hard (16 %), hard (48 %), and very hard (36 %) during the post-monsoon period (Table 3).

Table 3. Groundwater classifications on the basis of TDS Freeze and Cherry [27]; Davis and Dewiest [26] and TH Sawyer and McCarthy [29].

Parameters	Range	Water type/Classification	% of groundwater samples pre-monsoon	% of groundwater samples post-monsoon
TDS (mg/L)	<1000	Fresh	75	73
	1000-10000	Brackish	25	27
	10000-100000	Saline	-	-
	>100000	Brine	-	-
TH (mg/L)	<75	Soft	-	Nil
	75-150	Moderately hard	Nil	2
	150-300	Hard	45	41
	>300	Very hard	55	57

3.4. *Nitrate contamination*

Nitrate concentrations in groundwater have increased markedly in recent decades due to expanding urban settlements intensified industrial activity, and excessive application of nitrogen-based fertilizers. Elevated nitrate in potable water is recognized as a serious public health concern [30].

In the present investigation, nitrate concentrations ranged from 3 to 230 mg/L (average: 56 mg/L) during the pre-monsoon and from 5 to 797 mg/L (average: 63 mg/L) during the post-monsoon season (Table 2; Fig. 3). Spatial analysis indicated that 36 % of pre-monsoon samples and 40 % of post-monsoon samples exceeded the BIS permissible limit of 45 mg/L [24] (Fig. 4).

Nitrate enrichment in groundwater arises from a combination of natural and human-induced processes. Agricultural activities, including intensive farming and horticulture, along with discharge of domestic sewage and industrial effluents, have been widely recognized as major nitrate sources [31]. The extensive use of fertilizers such as urea, diammonium phosphate, and superphosphate further accelerates nitrate leaching from soils into groundwater systems [32]. Additional contributions originate from shallow aquifer recharge, improper solid waste disposal, livestock waste, and horticultural residues [33].

3.5. *Fluoride contamination*

The recommended maximum concentration of fluoride in drinking water is 1.0 mg/L, as stipulated by BIS [24] and the WHO [34], since prolonged exposure to elevated fluoride levels can result in dental and skeletal fluorosis [3]. In the study area, fluoride concentrations varied from 0.21 to 3.03 mg/L (mean: 1.20 mg/L) during the pre-monsoon and from 0.28 to 5.94 mg/L (mean: 1.28 mg/L) during the post-monsoon season. Exceedance of the acceptable limit was observed in 64 % of pre-monsoon and 59 % of post-monsoon samples (Table 2; Fig. 5).

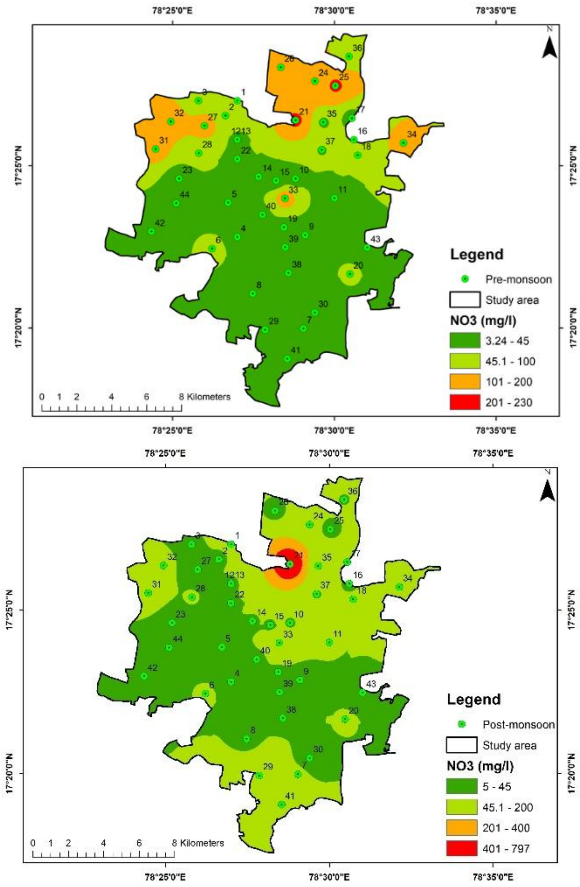

Fig. 3. Spatial distribution of NO_3^- concentration map in the pre-and post-monsoon seasons.

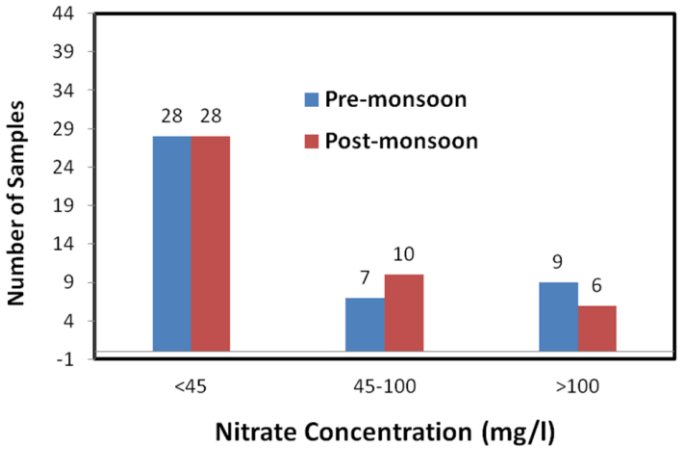

Fig. 4. Nitrate concentration for risk evaluation for drinking water in pre- and post-monsoon seasons.

Spatial distribution maps (Fig. 6) highlighted prominent fluoride-enriched zones in the northern, southern, and southwestern sectors of the study area. The alkaline nature of groundwater facilitates anion exchange and desorption mechanisms, thereby enhancing fluoride mobilization within the aquifer system [35].

Petrographic observations of granitic rocks confirm a predominantly geogenic source of fluoride. Euhedral zircon grains with compositional zoning were identified as inclusions within feldspar phenocrysts. Needle-shaped apatite aggregates were commonly observed in altered plagioclase and orthoclase minerals, while fluorite occurred as coarse-grained anhedral crystals. These fluoride-bearing mineral phases serve as the principal contributors to fluoride release into groundwater through prolonged water–rock interaction processes (Fig. 7).

Health assessments conducted in the study area revealed a notable occurrence of fluorosis-related symptoms among residents, indicating drinking water as the primary exposure pathway. These findings underline the necessity for immediate groundwater quality management measures and the implementation of safe drinking water alternatives in fluoride-affected regions.

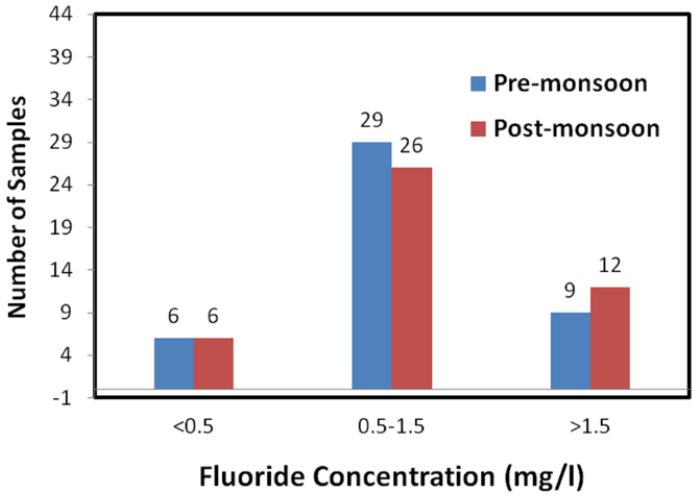

Fig. 5. Fluoride concentration for risk evaluation for drinking water in pre- and post-monsoon seasons.

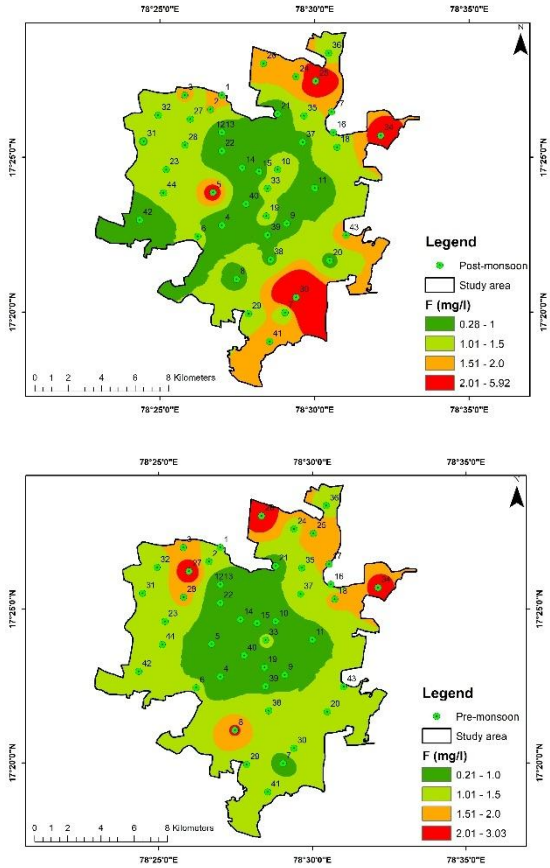

Fig. 6. Spatial distribution of fluoride concentration map in the pre- and post-monsoon seasons.

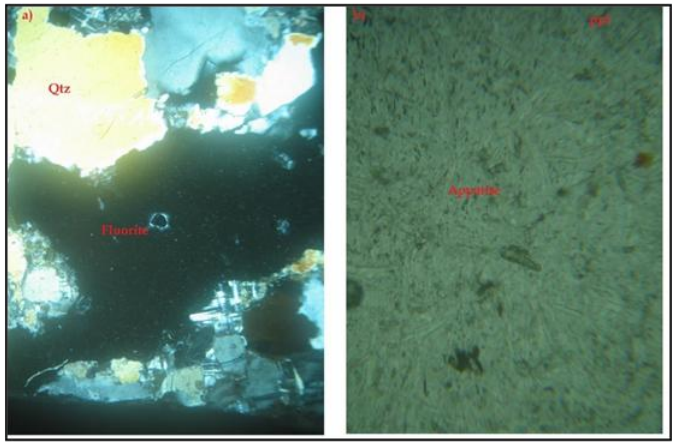

Fig. 7. Microphotographs of (a) Coarse-grained fluorite mineral associated with quartz and feldspar and (b) altered apatite in plane polarized light.

3.6. *Hydrochemical facies*

The Piper trilinear diagram [36] was employed to interpret the hydrochemical nature of groundwater and to identify dominant water types by integrating the relative proportions of major cations and anions within two triangular fields and a central diamond-shaped plot. This method enables a clear differentiation of groundwater facies and provides insights into the governing geochemical processes. Based on the Piper classification, groundwater samples from the study area were grouped into six distinct hydrochemical facies during both pre- and post-monsoon seasons.

The identified facies include Ca–HCO_3, Na–Cl, mixed Ca–Na–HCO_3, mixed Ca–Mg–Cl, and Ca–Cl types, occurring in varying proportions across the two seasons. The Piper plot (Fig. 8) indicates that groundwater chemistry is predominantly controlled by Ca–Na–HCO_3–Cl and Na–HCO_3–Cl facies, followed by mixed Na–Ca–Mg–HCO_3–Cl water types. Overall, the hydrochemical facies analysis demonstrates that fluoride enrichment in groundwater is governed not only by lithological composition but also by dynamic geochemical mechanisms such as alkali–alkaline earth ion exchange, dissolution of fluoride-rich minerals, and human-induced contamination.

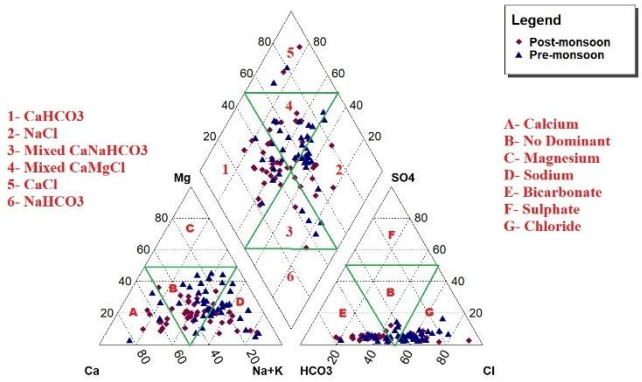

Fig. 8. Piper trilinear diagram in pre- and post-monsoon seasons.

3.7. *Gibbs diagram*

To identify the principal mechanisms controlling groundwater chemistry, Gibbs diagrams [37] were constructed by plotting total dissolved solids (TDS) against $Na^+/(Na^+ + Ca^{2+})$ and $Cl^-/(Cl^- + HCO_3^-)$ ratios, expressed in milliequivalents per liter. The Gibbs framework categorizes groundwater into precipitation dominance, rock dominance, and evaporation dominance zones, representing the relative influence of atmospheric inputs, lithological control, and evaporative concentration, respectively.

In the present study, the anionic ratio $[Cl^-/(Cl^- + HCO_3^-)]$ ranged from 0.15 to 0.85 (mean: 0.46) during the pre-monsoon and from 0.31 to 0.90 (mean: 0.57) during the post-monsoon season. Similarly, the cationic ratio $[(Na^+ + K^+)/(Na^+ + K^+ + Ca^{2+})]$ varied between

0.18–0.79 (mean: 0.46) in the pre-monsoon and 0.16–0.86 (mean: 0.48) in the post-monsoon season (Table 2). The majority of groundwater samples plot within the rock dominance field (Fig. 9), indicating that groundwater chemistry is primarily regulated by water–rock interaction processes, particularly silicate and feldspar weathering. This observation is consistent with the regional geology, which is dominated by granitic gneisses contributing major ions to groundwater through prolonged geochemical interaction.

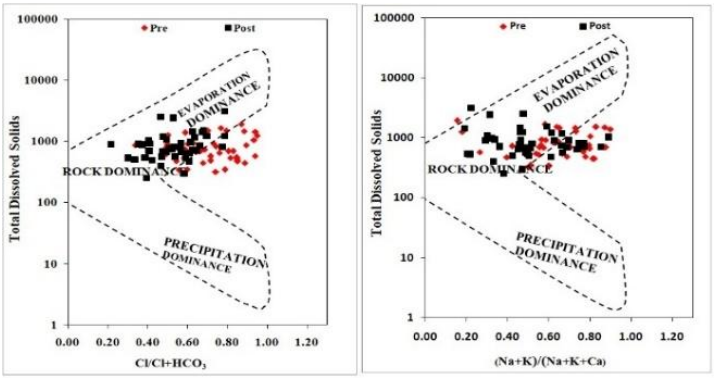

Fig. 9. Gibb's plot from the study area is rock-dominant factor controlling the groundwater chemistry in pre- and post-monsoon seasons.

3.8. *Ionic relationships and scatter plot analysis*

Scatter plot analysis was conducted to elucidate hydrogeochemical processes and ionic interrelationships controlling groundwater composition in the study area. Several diagnostic plots were examined to interpret mineral dissolution, ion exchange, and weathering mechanisms.

The plot of (Ca^{2+} + Mg^{2+}) versus (HCO_3^- + SO_4^{2-}) shows that most samples cluster near the equiline, suggesting that carbonate dissolution and silicate weathering are major contributors to groundwater chemistry (Fig. 10a). The relative contribution of alkali metals is highlighted in the (Na^+ + K^+)/total cation plot, which indicates the dominance of sodium and potassium derived mainly from silicate mineral breakdown (Fig. 10b).

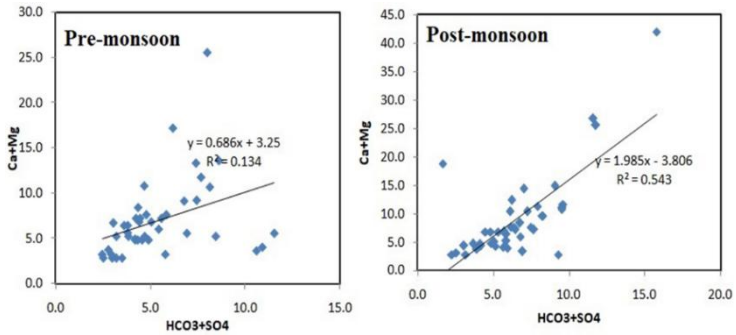

Fig. 10a. Scatter plot Ca+Mg vs HCO_3+SO_4 in pre- and post-monsoon seasons.

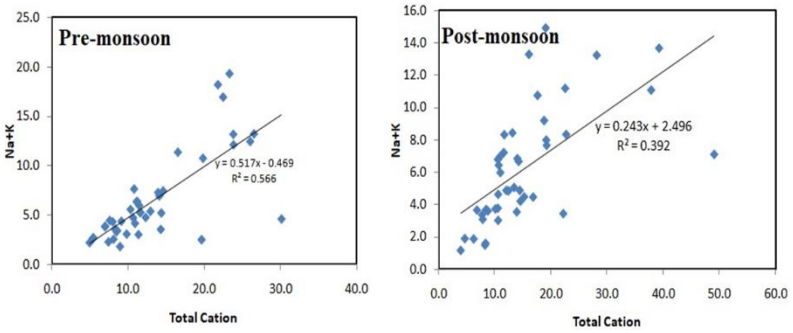

Fig. 10b. Scatter plot Na+K vs total cation in pre- and post-monsoon seasons.

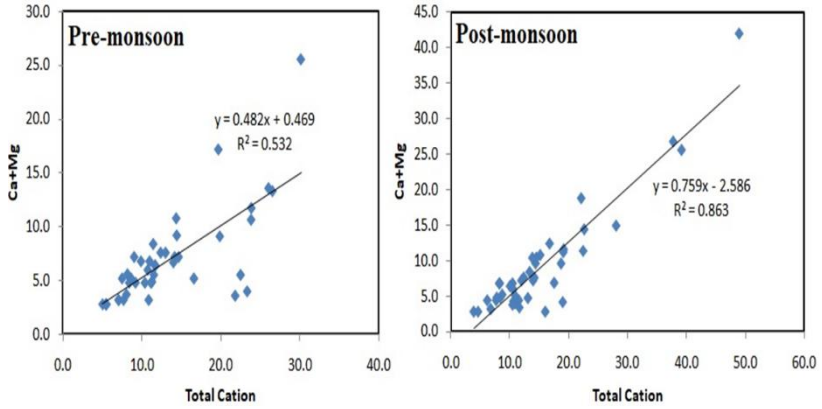

Fig. 10c. Scatter plot Ca+Mg vs total cation in pre- and post-monsoon seasons.

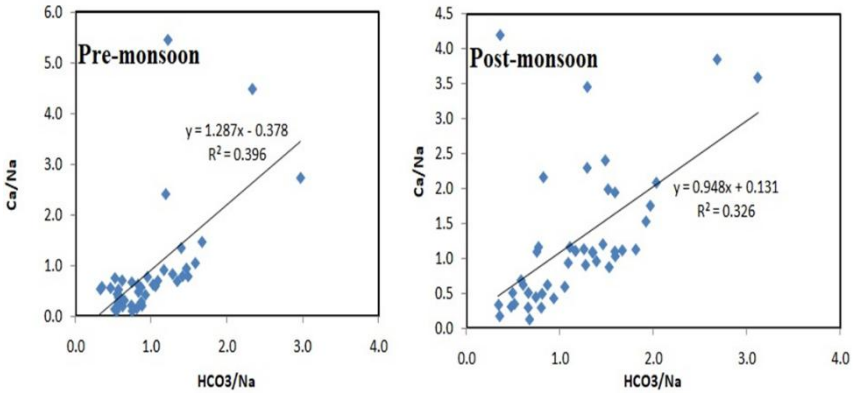

Fig. 10d. Scatter plot Ca/Na vs HCO3/Na in pre- and post-monsoon seasons.

A strong linear relationship between (Ca^{2+} + Mg^{2+}) and total cations further confirms the dominant role of alkaline earth metals in defining groundwater chemistry (Fig. 10c). Additionally, the Ca^{2+}/Na^{+} versus HCO_3^{-}/Na^{+} plot reveals trends characteristic of silicate

weathering coupled with ion exchange processes, with only a minor influence from carbonate dissolution (Fig. 10d).

Collectively, these scatter plots demonstrate that groundwater chemistry is largely controlled by the granitic nature of the aquifer matrix, where silicate mineral dissolution and cation exchange processes exert a strong influence on ionic composition [38–40].

3.9. *Multivariate factor analysis*

To identify the dominant processes influencing groundwater chemistry and reduce dataset complexity, factor analysis was performed using SPSS version 23 with varimax rotation. Factors with eigenvalues greater than 1.0 were retained. During the pre-monsoon season, four principal components were extracted, collectively accounting for 80.43 % of the total variance (Table 4a; Fig. 11a). Factor loadings were interpreted as strong (>0.75), moderate (0.50–0.75), or weak (0.30–0.50), following Mor *et al*. [41].

Factor 1 explains 31.54 % of the variance and exhibits strong positive loadings for Cl^-, Ca^{2+}, total hardness (TH), SO_4^{2-}, EC, and TDS, indicating the combined influence of mineral dissolution, carbonate weathering, and salinity enrichment. Factor 2 accounts for 23.06 % of the variance and is characterized by high loadings of Na^+, HCO_3^-, F^-, and TDS, reflecting fluoride mobilization from fluoride-bearing minerals under alkaline conditions. Factor 3 (14.25 % variance) shows strong loadings on pH, CO_3^{2-}, and K^+, suggesting alkaline buffering effects and contributions from potassium-bearing minerals. Factor 4 (10.62% variance) is dominated by NO_3^- and Mg^{2+}, indicating anthropogenic influences such as fertilizer application and sewage infiltration.

During the post-monsoon season, four significant factors explained 75.71 % of the total variance (Table 4b; Fig. 11b). Factor 1 (35.15 %) shows strong loadings on Mg^{2+}, EC, Cl^-, Ca^{2+}, and HCO_3^-, reflecting ion exchange, silicate weathering, and anthropogenic impacts. Factor 2 (15.35 %) is dominated by NO_3^- and SO_4^{2-}, with a negative association with fluoride, indicating competitive geochemical behavior influenced by agricultural inputs. Factor 3 (15.19 %) exhibits strong loadings on pH, TH, and CO_3^{2-}, highlighting the role of carbonate mineral dissolution under variable pH conditions. Factor 4 (7.99 %) is characterized by Na^+ enrichment and inverse K^+ loading, suggesting plagioclase feldspar weathering and possible industrial contributions.

Table 4a. Principal component analysis on groundwater data in pre-monsoon season.

Parameters	Principal Component Analysis In pre-monsoon			
	PC1	PC2	PC3	PC4
Cl^-	**0.898**	0.279	-0.134	0.143
Ca^{2+}	**0.892**	-0.051	-0.239	0.048
TH	**0.870**	-0.024	-0.269	0.333
SO_4^{2-}	**0.823**	0.142	0.074	-0.243
Cond	**0.752**	**0.614**	-0.099	0.191
TDS	**0.752**	**0.614**	-0.099	0.191
Na^+	0.256	**0.898**	0.097	-0.013
HCO_3^-	0.267	**0.858**	-0.216	0.081

F^-	-0.096	**0.725**	-0.118	0.123
pH	-0.199	0.109	**0.887**	-0.078
CO_3^{2-}	-0.098	-0.338	**0.843**	-0.008
K^+	-0.119	-0.077	**0.465**	0.443
Mg^{2+}	0.157	0.063	-0.141	**0.798**
NO_3^-	0.113	0.412	0.137	**0.599**
Eigen Value	4.415	3.229	1.994	1.486
% of Variance	31.535	23.063	14.245	10.615
Cumulative % of variance	31.535	54.598	68.843	79.458

Table 4b. Principal Component analysis on groundwater data in post-monsoon season.

Parameters	Principal Component Analysis In post-monsoon			
	PC1	PC2	PC3	PC4
Mg^{2+}	**0.964**	-0.120	0.060	-0.019
Cond.	**0.934**	0.295	-0.128	0.116
TDS	**0.934**	0.295	-0.128	0.116
Cl^-	**0.929**	0.105	0.096	0.132
Ca^{2+}	**0.823**	0.363	-0.199	-0.053
HCO_3^-	**0.556**	0.138	-0.474	0.312
NO_3^-	0.236	**0.830**	-0.166	0.015
SO_4^{2-}	0.399	**0.814**	-0.163	0.158
F^-	0.033	**-0.518**	-0.230	0.270
pH	-0.069	-0.067	**0.851**	0.145
CO_3^{2-}	-0.108	0.087	**0.743**	-0.221
TH	0.082	-0.121	**0.650**	0.318
K^+	0.023	0.152	-0.102	**-0.788**
Na^+	0.396	0.358	0.019	**0.607**
Eigen Value	4.921	2.148	**2.126**	1.405
% of Variance	35.147	15.346	**15.186**	10.032

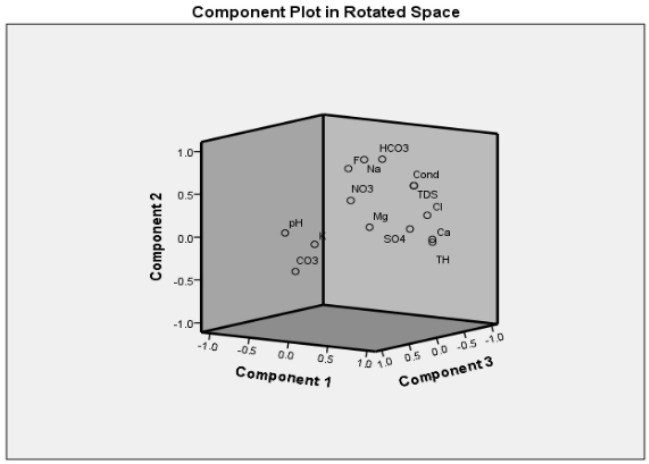

Fig. 11a. Principal component plot in rotated space groundwater data in the pre-monsoon.

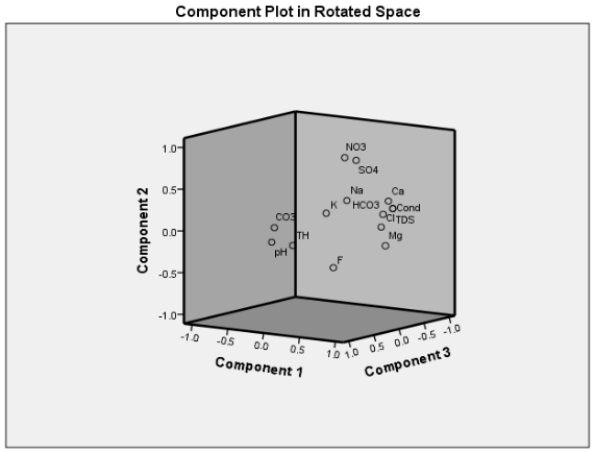

Fig. 11b. Principal component plot in rotated space surface water samples in the post-monsoon season.

3.10. *Non-carcinogenic health risk assessment*

The potential non-carcinogenic health risks associated with fluoride (F^-) and nitrate (NO_3^-) ingestion through drinking water were evaluated for adults and children during both seasons using hazard quotient (HQ) and total hazard index (THI) models.

For adults, HQ values during the pre-monsoon ranged from 0.13–1.94 (mean: 0.77) for fluoride and 0.07–5.54 (mean: 1.34) for nitrate. During the post-monsoon, HQ values varied between 0.18–3.81 (mean: 0.82) for fluoride and 0.13–19.16 (mean: 1.53) for nitrate (Tables 5a and 5b).

For children, fluoride HQ values ranged from 0.18–2.63 (mean: 1.04) and nitrate from 0.10–7.49 (mean: 1.81) in the pre-monsoon season. Post-monsoon HQ values increased to 0.24–5.15 (mean: 1.11) for fluoride and 0.18–25.91 (mean: 3.78) for nitrate. According to US EPA guidelines [8], HQ values exceeding unity indicate potential non-carcinogenic health risk.

During the pre-monsoon, approximately 52 % of samples exceeded HQ = 1 for children, while exceeded for adults were 21 % (fluoride) and 43 % (nitrate). In the post-monsoon season, HQ exceeded increased to 48 % (fluoride) and 66 % (nitrate) for children, and 27 % and 43 % for adults, respectively.

The combined health risk, expressed as THI, ranged from 0.36–6.75 (mean: 2.27) in the pre-monsoon and 0.38–19.38 (mean: 2.79) in the post-monsoon for adults. For children, THI values ranged from 0.49–9.12 (mean: 3.07) and 0.52–26.21 (mean: 3.78) in the respective seasons (Fig. 12a,b). These results clearly indicate significant non-carcinogenic health risks associated with fluoride and nitrate exposure, with children being the most vulnerable population group in the study area.

Table 5a. Hazard Quotient (HQ) and Total Hazard Index (THI) for adults and children in the study area of pre-monsoon season.

Sample No.	HQ of F^- in adult	HQ of NO_3^- in adult	THI	HQ of F^- in children	HQ of NO_3^- in children	THI
1	0.63	1.08	1.72	0.86	1.46	2.32
2	0.82	1.29	2.11	1.11	1.75	2.86
3	1.16	0.99	2.15	1.57	1.34	2.91
4	0.27	0.09	0.36	0.36	0.12	0.49
5	0.41	0.11	0.52	0.55	0.14	0.70
6	0.70	1.92	2.62	0.94	2.59	3.54
7	0.47	0.60	1.07	0.63	0.81	1.45
8	1.35	0.13	1.48	1.83	0.17	2.00
9	0.55	0.07	0.63	0.75	0.10	0.85
10	0.53	0.54	1.06	0.71	0.72	1.43
11	0.42	0.10	0.52	0.57	0.14	0.71
12	0.15	0.79	0.94	0.21	1.06	1.27
13	0.13	0.82	0.96	0.18	1.11	1.29
14	0.21	0.73	0.94	0.29	0.99	1.27
15	0.31	0.09	0.40	0.42	0.12	0.54
16	0.78	1.10	1.88	1.06	1.48	2.54
17	1.22	0.39	1.62	1.66	0.53	2.19
18	1.06	1.59	2.64	1.43	2.15	3.58
19	0.57	0.64	1.21	0.77	0.86	1.63
20	0.76	1.30	2.07	1.03	1.76	2.79
21	0.43	5.54	5.97	0.58	7.49	8.07
22	0.28	0.67	0.96	0.38	0.91	1.29
23	0.68	0.10	0.78	0.92	0.13	1.05
24	0.83	2.93	3.76	1.12	3.97	5.08
25	1.26	5.48	6.75	1.71	7.41	9.12
26	1.88	2.77	4.65	2.54	3.74	6.28
27	1.94	4.04	5.98	2.63	5.46	8.09
28	1.08	1.12	2.20	1.46	1.51	2.98
29	0.88	0.48	1.36	1.19	0.65	1.84
30	0.78	0.25	1.03	1.06	0.34	1.40
31	0.74	3.41	4.15	1.00	4.62	5.61
32	0.64	3.83	4.47	0.87	5.18	6.05
33	0.76	4.04	4.79	1.02	5.46	6.48
34	1.44	3.19	4.63	1.94	4.32	6.26
35	0.77	0.85	1.62	1.04	1.15	2.19
36	0.87	1.35	2.22	1.18	1.82	3.00
37	0.74	1.01	1.75	1.00	1.37	2.36
38	0.85	1.06	1.91	1.14	1.44	2.58
39	0.60	0.85	1.45	0.81	1.15	1.97
40	0.42	0.79	1.21	0.56	1.07	1.64
41	0.89	0.12	0.36	1.20	0.16	0.49
42	0.89	0.10	6.75	1.20	0.13	9.12
43	0.80	0.45	2.21	1.08	0.61	2.99
44	0.82	0.24	2.18	1.11	0.33	2.95

Table 5b. Hazard Quotient (HQ) and Total Hazard Index (THI) for Adults and Children in the study area of post-monsoon season.

Sample No.	HQ of F^- in adult	HQ of NO_3^- in adult	THI	HQ of F^- in children	HQ of NO_3^- in children	THI
1	1.17	1.05	2.22	1.58	1.43	3.00
2	1.00	0.90	1.90	1.35	1.22	2.57
3	1.01	0.86	1.86	1.36	1.16	2.52
4	0.24	0.14	0.38	0.32	0.20	0.52
5	1.60	0.53	2.13	2.16	0.72	2.88
6	0.69	1.41	2.10	0.94	1.91	2.84
7	0.54	1.27	1.81	0.73	1.71	2.44
8	0.53	0.46	0.99	0.71	0.63	1.34
9	0.51	0.24	0.75	0.69	0.33	1.02
10	0.95	0.85	1.79	1.28	1.14	2.43
11	0.34	1.18	1.53	0.46	1.60	2.06
12	0.28	1.25	1.52	0.37	1.69	2.06
13	0.34	0.84	1.18	0.46	1.14	1.60
14	0.18	0.87	1.04	0.24	1.17	1.41
15	0.53	0.82	1.35	0.72	1.10	1.82
16	0.78	0.53	1.31	1.06	0.72	1.78
17	1.03	2.85	3.88	1.39	3.86	5.24
18	0.91	1.20	2.11	1.23	1.63	2.86
19	0.79	0.92	1.71	1.07	1.25	2.31
20	0.54	1.25	1.79	0.72	1.69	2.41
21	0.22	19.16	19.38	0.30	25.91	26.21
22	0.21	0.60	0.81	0.28	0.81	1.09
23	0.86	0.13	0.99	1.16	0.18	1.34
24	1.03	1.66	2.69	1.40	2.24	3.63
25	2.31	0.22	2.53	3.12	0.30	3.42
26	1.14	0.30	1.44	1.54	0.41	1.95
27	0.89	0.43	1.32	1.20	0.58	1.78
28	0.76	1.21	1.98	1.03	1.64	2.67
29	0.72	4.81	5.52	0.97	6.50	7.47
30	3.81	0.44	4.25	5.15	0.60	5.75
31	0.63	2.60	3.22	0.85	3.51	4.36
32	0.82	1.32	2.14	1.11	1.78	2.89
33	0.76	4.04	4.79	1.02	5.46	6.48
34	1.58	3.44	5.02	2.13	4.65	6.78
35	0.67	1.22	1.89	0.91	1.65	2.56
36	0.71	1.01	1.71	0.95	1.37	2.32
37	0.51	0.87	1.38	0.69	1.17	1.86
38	0.59	0.92	1.51	0.80	1.24	2.04
39	0.56	0.91	1.48	0.76	1.24	2.00
40	0.27	0.63	0.89	0.36	0.85	1.21
41	1.10	1.06	0.38	1.49	1.44	0.52
42	0.37	0.19	19.38	0.50	0.26	26.21
43	1.12	0.34	2.46	1.51	0.46	3.32
44	0.67	0.19	2.41	0.91	0.26	3.26

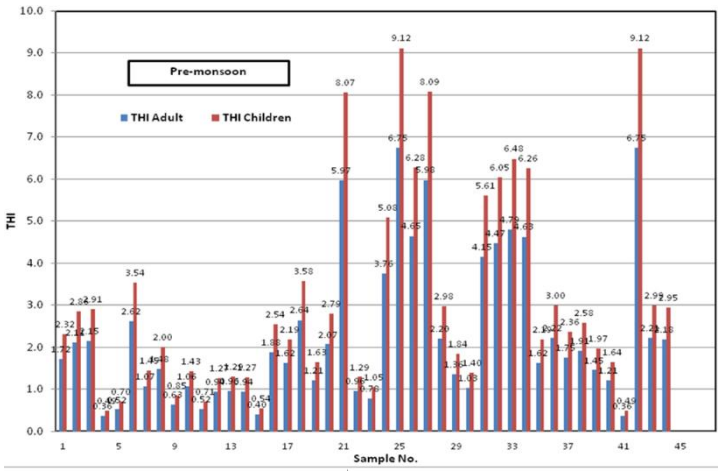

Fig. 12a. Total Hazard Index of adult and children in the pre-monsoon season.

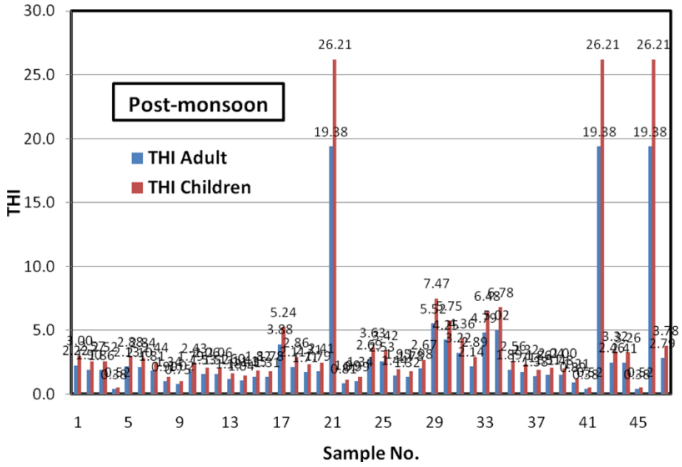

Fig. 12b. Total Hazard Index of adult and children in the post-monsoon season.

4. Conclusions

The groundwater in the study region is slightly alkaline. High fluoride concentrations were observed in the south-western, northern, and central parts, reflecting the predominance of F^--rich minerals in the granitic terrain. Elevated nitrate levels indicate that fertilizers and domestic sewage contribute to groundwater contamination. Hydrochemical facies analysis using the Piper diagram revealed that Ca–HCO_3, NaCl, and Mixed Ca–Na–HCO_3 types dominate during both pre- and post-monsoon seasons, reflecting the influence of rock weathering and mineral dissolution. Gibbs diagram analysis indicated that groundwater chemistry is largely controlled by rock–water interaction, with only a few areas affected by evaporation. Factor analysis identified four principal components controlling groundwater quality, highlighting the combined influence of silicate mineral weathering, cation

exchange, and anthropogenic activities. Health risk assessment showed that the hazard quotients for fluoride and nitrate exceeded the USEPA non-carcinogenic threshold of 1.0 for both children and adults, indicating that children are more vulnerable to groundwater contamination in the study region. Overall, groundwater quality is primarily influenced by natural geochemical processes and human activities, posing significant health risks that require targeted management interventions.

Acknowledgment

We are thankful to the Department of Geology, Osmania University Hyderabad, for providing laboratory facilities.

References

1. B. M. Reddy and V. Sunitha, Environ. Chem. Ecotoxicol. **2**, 150 (2020). https://doi.org/10.1016/j.enceco.2020.09.002
2. U.S. Environmental Protection Agency (EPA). Risk Assessment Guidance for Superfund (RAGS), Volume I: Human Health Evaluation Manual (Part E, Supplemental Guidance/or Dermal Risk Assessment), Final. Office of Superfund Remediation and Technology Innovation. Washington, DC. July (2004).
3. E. Satyanarayana, R. Dhakate, D. L. Kumar, P. Ravindar, and M. Muralidhar, J. Geol. Soc. India **89**, 247 (2017). https://doi.org/10.1007/s12594-017-0597-8
4. Y. Zhang, J. Wu, and B. Xu, Environ. Earth Sci. **77**, 273 (2018). https://doi.org/10.1007/s12665-018-7456-9
5. V. B. Sunitha, M. R. Reddy, and M. R. Reddy, Int. J. Res. Chem. Environ. **2**, 88 (2012). https://doi.org/10.1016/j.enceco.2020.09.002
6. A. Kadam, V. Wagh, and B. Umrikar, Environ. Dev. Sustain. **22**, 7033 (2020). https://doi.org/10.1007/s10668-019-00527-w
7. S. More, R. Dhakate, G. V. Ratnalu, and G. Machender, Environ. Earth Sci. **80**, 262 (2021). https://doi.org/10.1007/s12665-021-09544-3
8. USEPA, Human Health Evaluation Manual, Supplemental Guidance: Update of Standard Default Exposure Factors, OSWER Directive 9200.1-120 (United States Environmental Protection Agency, Washington, 2014).
9. S. He and J. Wu, Expo. Health. **11**, 125 (2019). https://doi.org/10.1007/s12403-018-0289-7
10. V. M. Wagh, D. B. Panaskar, S. V. Mukate, M. L. Aamalawar, and U. L. Sahu, Hum. Ecol. Risk Assess. **26**, 654 (2019). https://doi.org/10.1080/10807039.2018.1528861
11. D. Karunanidhi, P. Aravinthasamy, T. Subramani, J. Wu, and K. Srinivasamoorthy, Hum. Ecol. Risk Assess. **25**, 250 (2019). https://doi.org/10.1080/10807039.2019.1568859
12. S. Gugulothu, N. S. Rao, R. Das, D. L. Kumar, and D. Ratnakar, Environ. Sci. Pollut. Res. **29**, 49070 (2022). https://doi.org/10.1007/s11356-022-18967-9
13. N. S. Rao, B. Ravindra, and J. Wu, Hum. Ecol. Risk Assess. **26**, 2316 (2020). https://doi.org/10.1080/10807039.2020.1741338
14. S. Ayoob and A. Gupta, Crit. Rev. Environ. Sci. Technol. **36**, 433 (2006). https://doi.org/10.1080/10643380600678112
15. A. Narsimha and S. Rajitha, Hum. Ecol. Risk Assess. **24**, 2119 (2018). https://doi.org/10.1080/10807039.2018.1438176
16. D. Karunanidhi, P. Aravinthasamy, T. Subramani, P. D. Roy, and K. Srinivasamoorthy, Nat. Resour. Res. **29**, 2369 (2020). https://doi.org/10.1007/s11053-019-09592-4
17. L. Yuan, W. Fei, F. Jia, J. P. LV, Qi. Liu, F-r. Nan, X.-D. Liu, and S.-L. Xie, Chemosphere **243**, ID 125451 (2020). https://doi.org/10.1016/j.chemosphere.2019.125451

18. M. S. Zango, E. D. Sunkari, M. Abu, and A. Lermi, J. Geochem. Explor. **207**, ID 106363, (2019). https://doi.org/10.1016/j.gexplo.2019.106363
19. CGWB, Central Ground Water Board, Ministry of Water Resources, Government of India, Ground Water Brochure, Mahabubnagar District, Nizamabad District, Khammam District; Hyderabad, India (2013).
20. APHA, Standard methods for the examination of water and wastewater, 22nd Edition (American Public Health Association, Washington, DC, USA, 2012).
21. P. Li, R. Tian, and R. Liu, Expo. Health, **11**, 81 (2019). https://doi.org/10.1007/s12403-018-0277-y
22. K. Brindha, R. Paul, J. Walter, M. L. Tan, M. K. Singh, Environ. Geochem. Health. **42**, 3819 (2020). https://doi.org/10.1007/s10653-020-00637-9
23. USEPA, USEPA Region III Risk-based Concentration Table: Technical Background Information (United States Environmental Protection Agency, Washington, 2006).
24. BIS, Second Revision Bureau of Indian Standards, Drinking Water Sectional Committee, FAD 25 New Delhi, India. ISO: 10500 (2012).
25. K. Brindha and R. Kavitha, Environ. Earth Sci. **73**, 5383 (2015). https://doi.org/10.1007/s12665-014-3793-5
26. S. N. Davis and R. J. M. Dewiest, Hydrogeology (John Wiley and Sons Inc, NY, 1966).
27. R. A. Freeze and J. A. Cherry, Groundwater (Prentice Hall Inc, New Jersey, 1979).
28. S. A. Ali and U. Ali, Appl. Water Sci. **8**, 1 (2018). https://doi.org/10.1007/s13201-018-0678-x
29. C. N. Sawyer, P. L. Mccarty, and G. F. Parkin, Chemistry for Environmental Engineering and Science, 5th Edition (McGraw-Hill, New York, 2003).
30. E. Allam, H. K. Gangula, R. Arukonda, and M. Muralidhar, Data Brief, **33**, ID 106462 (2020). https://doi.org/10.1016/j.dib.2020.106462
31. O. Oenema, L. V. Liere, and O. Schoumans, J. Hydrol. **304**, 289 (2005). https://doi.org/10.1016/j.jhydrol.2004.07.044
32. M. Jalali, Environ. Earth. Sci. **62**, 907 (2011). https://doi.org/10.1007/s12665-010-0576-5
33. L. Lokesh, Asian J. Water Environ. Pollut. **10**, 91 (2013). https://doi.org/10.3233/AJW-2013-10_2_13
34. World Health Organization, Guidelines for Drinking Water Quality, 4th Edition (World Health Organization, Geneva, 2011).
35. V. K. Saxena and S. Ahmed, Environ. Geol. **43**, 731 (2003). https://doi.org/10.1007/s00254-002-0672-2
36. A. M. Piper, Trans. Am. Geophys. Union. **25**, 914 (1944).
37. R. J. Gibbs, Science **170**, 795 (1970). https://doi.org/10.1126/science.170.3962.1088
38. D. L. Kumar, E. Satyanarayana, R. Dhakate, and P. R. Saxena, Groundw. Sustain. Dev. **8**, 474 (2019). https://doi.org/10.1016/j.gsd.2019.01.008
39. A. Edukondal, L. Kumar, M. Ramu, G. Harikrishna, and M. Muralidhar, Environ. Sci. Pollut. Res. **29**, 72344 (2022). https://doi.org/10.1007/s11356-022-18517-3
40. L. K. Duvva, K. K. Panga, R. Dhakate, and V. Himabindu, Appl. Water Sci. **12**, 11 (2022). https://doi.org/10.1007/s13201-021-01557-4
41. S. Mor, K. Ravindra, R. P. Dahiya, and A. Chandra, Environ. Monit. Assess. **118**, 435 (2006). https://doi.org/10.1007/s10661-006-1505-7